Draft version December 7, 2024
Typeset using LaTeX **twocolumn** style in AASTeX631

Deformation and differential rotation in slowly rotating young intermediate-mass stars

Subrata Kumar Panda [1] and Shravan Hanasoge [1]

[1] *Department of Astronomy and Astrophysics, Tata Institute of Fundamental Research, Colaba, Mumbai 400005, Maharashtra, India*

ABSTRACT

Asteroseismology, the study of stellar vibrations, is a method with which to probe small-scale deformations in stellar shapes and their subsurface rotation profiles. Salient among the seismic inferences of rotation from TESS observations are TIC 408165734, whose equatorial rotation rate is 10% faster than the pole, and TIC 307930890, which has significant radial shear and shows a decreasing spin rate outward through its envelope. We also measure structural deformation in fifteen stars, nine of which are oblate, a finding consistent with expectations for relatively fast-rotating, non-magnetic stars. The difference between polar and equatorial radii in TIC 47639058 is 130 times larger than that for the Sun. The remaining six stars display a surprising prolate shape, suggesting the presence of equatorial toroidal magnetic fields and challenging the idea that δ Scutis are non-magnetic. These inferences provide constraints for numerical simulations and new insights to guide theories of δ Scuti structure and rotation.

1. INTRODUCTION

Rotation profoundly influences stellar evolution, structure and dynamics. One major effect, especially in fast rotators, is deformation, which turns the stars into ellipsoids, in turn leading to phenomena such as gravity darkening (von Zeipel 1924; Espinosa Lara, F. & Rieutord, M. 2011), enhanced accretion efficiencies (Hastings, B. et al. 2021), anisotropic winds (Hastings, B. et al. 2023) and mass-loss episodes (Gagnier, D. et al. 2019). In binary systems, deformation can impact the tidal interaction, exchange of angular momenta, and energy dissipation (Song, H. F. et al. 2017; Damiani, C. & Mathis, S. 2018) between the bound objects. Differential (non-rigid) rotation of stars affects interior mixing processes (Koenigsberger, G. et al. 2021) and prolongs their main-sequence lifetimes by supplying additional Hydrogen to the cores. Rotational shear, as in the case of the Sun, amplifies magnetic field by twisting field lines (Zahn, J.-P. et al. 2007), with kinetic energy being converted to magnetic energy. Differential rotation also generates toroidal magnetic field by winding up the poloidal components (Machida et al. 2007), resulting in increased Lorentz stresses, in turn acting to suppress differential rotation (Fuller et al. 2019). The interplay between stellar evolution and angular momentum transport (magnetic torque, rotational instability, internal gravity waves) collectively determines the core-to-surface rotation gradient, which has been measured in numerous stars using methods of asteroseismology (Aerts et al. 2010; Benomar et al. 2015; Reeth et al. 2015; Bowman 2020).

Non-radial modes of stellar oscillation may be used to infer differential rotation and magnetism, because they cause modes of specific angular degree ℓ to split into a set of $(2\ell+1)$ multiplets. These splittings have enabled the measurements of interior differential rotation (Mosser, B. et al. 2012) in 22% of red giant stars (Cantiello et al. 2014), demonstrating that their cores are spinning faster than the envelopes, but slower than theoretically expected (Belkacem, K. et al. 2015). Asteroseismic mode splittings also enable ensemble-scale inference of differential rotation in main-sequence stars (Bazot, M. et al. 2019; Benomar et al. 2018, 2023). Negligible differences between the core and envelope rotation rates of main-sequence stars align well with the expectation that they rotate nearly rigidly due to efficient angular momentum transport (Fuller et al. 2014). These stars rotate slowly and are nearly spherical in shape.

In contrast, hot stars of intermediate masses ($1.5 - 2.5 M_\odot$) known as δ Scutis, are rapid rotators ($\Omega \sim 10 - 100 \Omega_\odot$) and are consequently deformed - typically oblate in shape due to centrifugal forcing - in structure. Dynamo-generated magnetic fields are thought to be absent in them (Guzik 2021). Nevertheless, observations have revealed magnetic fields in some δ Scutis (Balona 2019; Zwintz, K. et al. 2020). The splittings of non-radial modes that provide insights into rotation and deviations are not easily identified in the oscillation spec-

tra of δ Scutis due to challenges in mode identification (Bedding et al. 2020). Notably in the case of star KIC 11145123, a relatively slowly spinning δ Scuti star, measurements of internal rotation (Kurtz et al. 2014) and ellipsoidal deformation (Gizon et al. 2016) were possible.

The measurement of deformation and differential rotation across a larger sample of δ Scutis is essential to understand the dynamics pertinent to this mass range and stellar class. With the availability of a large observational dataset from the TESS mission, and the discovery of many δ-Scuti pulsators with regularly patterned oscillation (Bedding et al. 2020, Singh et al. 2024), a group of 38 have been identified as showing rotational splittings, among which numerous instances show triplets (Singh et al. 2024). We analyzed all objects in this sample with the aim of discovering signatures of differential rotation and deformation in these stars.

2. RESULT

Following notation developed first in helioseismology, modes of azimuthal order m of a non-radial multiplet, with radial order n and degree ℓ are expressed in a basis of ζ polynomials (Schou et al. 1994), whose coefficients (the so-called a-coefficients, Ritzwoller & Lavely 1991) are quantities that may be directly related to perturbative contributions (equation 1) of axisymmetric but processes such as rotation and differential rotation, stellar deformation, and magnetism.

$$\nu_{n,\ell,m} = \nu_{n,\ell} + \sum_{j=1}^{j=2\ell} a_j(n,\ell)\ \zeta_j^{(\ell)}(m). \tag{1}$$

The a_1 coefficient serves as a proxy to the mean stellar rotation (Appourchaux, T. et al. 2014); higher odd a-coefficients, such as a_3, quantify the extent of latitudinal differential rotation, i.e., where the rotation rate changes as a function of latitude. Similarly, even coefficients, a_2 capture centrifugal and magnetism-induced deformation. At leading order, each of these coefficients is independent, allowing us to write a sequence of separate inverse problems.

2.1. *Radial Differential Rotation*

Since stellar cores shrink and envelopes swell during their evolution, the moments of inertia associated with the cores decline, causing them to spin faster than the envelopes. This leads to the emergence of a rotation gradient along the radial direction. Resonnant acoustic waves (p-modes) propagate in different geometric cavities within stars and by combining all the information they contain, it may be possible to infer details of the internal rotation profiles. Depending on the rotation rates at the regions where the mode eigenfunctions possess the largest amplitudes, the observed mode splittings can vary. Hence, the mean rotation rates $\langle f_{\rm rot}\rangle$ obtained from dipole-mode splitting generally varies with their radial orders. The coefficient a_1 serves as an indicator of this mean rotation, and may be obtained from the half-spacing between the $m = \pm 1$ modes (equation A10).

TIC 307930890 is the best candidate among our sample to demonstrate radial differential rotation, since it exhibits a continuous sequence of four rotationally split dipole doublets, whose frequency spacings gradually decrease across the radial orders (Fig. 1a). The apparent absence of the $m = 0$ components at all radial orders suggests either a high inclination angle or the involvement of a systematic mode-suppression mechanism in this star. It offers an ideal opportunity to probe the differential rotation profiles in the outer envelope of this star since the acoustic modes are predominantly sensitive to the near-surface regions (Fig. 1d) of δ Scuti stars.

The frequency splittings of dipole ($\ell = 1$) modes are written in terms of the first two a-coefficients (equation 2), of which we are interested in the rotation term, a_1. Using the MCMC method (see Appendix C) we fitted the dipole doublets at each radial order n with equation 2 in order to retrieve the a_1 coefficients. These coefficients effectively measure the mean rotation rates up to an additional factor involving the effect of Coriolis force, i.e., $(1 - C_L)\langle f_{\rm rot}\rangle$.

$$\nu_{n,1,m} = \nu_{n,1} + a_1 m + a_2(3m^2 - 2) \tag{2}$$

The best-fit model for TIC 307930890 (Singh et al. 2024) suggests this star has a mass of $1.7 M_\odot$, metallicity $Z = 0.018$, and an age of 17 Myr. Simulating a stellar model with these properties using `MESA` (Paxton et al. 2010, 2013, 2015, 2018, 2019) and performing a pulsation calculation with `GYRE` (Townsend & Teitler 2013; Townsend et al. 2017; Goldstein & Townsend 2020), we noticed the $\ell = 1$ frequencies of radial orders between 3 and 6 appear in the range of dipole modes observed in this star. Thus, we calculated the Ledoux constants C_L (equation A3) for these modes, and divided the a_1 coefficients by the factor $(1 - C_L)$ to retrieve rotation rates $\langle f_{\rm rot}\rangle$ (equation A1).

We demonstrate the radial order (n) dependence of $\langle f_{\rm rot}\rangle$ in Fig. 1(c), which depicts its descending nature with increasing radial order. Rotation kernels, which capture the sensitivities of the acoustic modes to the rotation rate as a function of radius, peak in the outermost

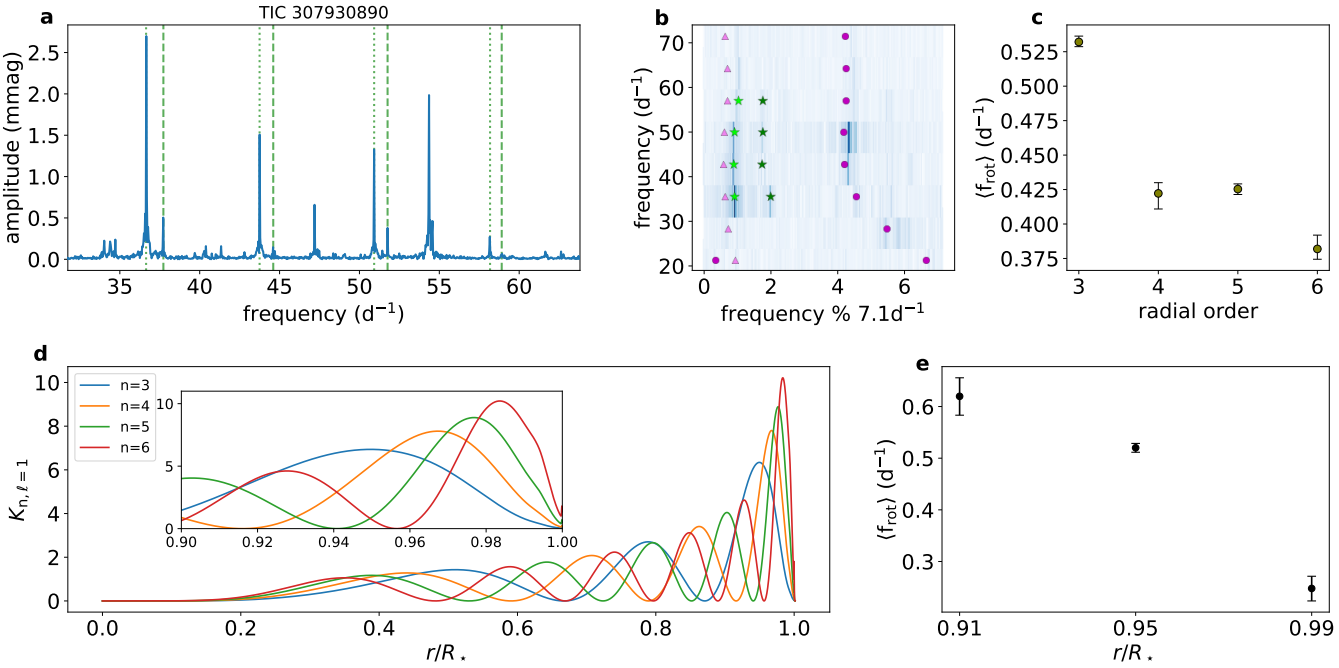

Figure 1. Radial differential rotation in a δ Scuti star. a. Power spectrum of TIC 307930890 with rotationally split dipole-mode ($\ell = 1$) doublets at four radial orders. The $m = -1$ ($+1$) components are marked with dotted (dashed) lines. **b.** The Échelle diagram associated with this spectrum, obtained by vertically stacking equal-width segments of oscillation spectra, which aligns the modes of a given harmonic degree (ℓ) into separate vertical ridges. The ridge on the right comprises $\ell = 0$ modes. The ridge on the left, appearing to be split into two columns, correspond to the $m = -1$ and $m = +1$ components of the dipole ($\ell = 1$) modes. The dipole doublets have been marked with stars symbols, while the circle and triangle symbols anchor the best fit model's radial and dipole modes respectively. **c.** Rotation rates obtained from the four dipole modes as a function of their radial order (n). **d.** Radial variation of rotation kernels of the four dipole modes. The kernel represents the modes' ability to sense stellar rotation at specific regions. The inset zooms into the outer 10% portion of the star, which shows that, lower the radial order, the deeper it probes. **e.** A three zone spatial analysis to decipher the crude trend of the rotational shear within outer 10% of envelope.

(**Figure set-1 available with the convergence plots obtained from several MCMC fittings.**)

layers of the envelope, where the modes spend most time (Fig. 1d). The sensitivity gradually increases toward the surface layers with growing radial order (see the zoomed inset). Thus, we expect an outwardly decreasing spin rate for this star. Obtaining a more informative spatial rotation profile for this star requires solving a kernel-weighted inverse problem (equation A5); however, since we only have a limited number of rotational splitting measurements (four radial orders), we are unable to improve the resolution. Because of the simplicity of the inverse problem, we proceed using a forward-modelling approach.

For the specific stellar model we analyzed here, all kernels appear to peak within the outer 10% of the envelope. The rotation profile is represented as 3 parameters at $r = \{0.91,\ 0.95,\ 0.99\}R_\star$. We sample the range of three-parameter choices that best fit the observed splittings using an MCMC-based search (see appendix D for details). The rotation frequencies of the best-fit model obtained at the aforementioned positions are shown in Figure 1(e), where the spin rates appear to decline radially outwards, indicating the presence of radial differential rotation.

2.2. *Deformation in Shape*

In the case of a slowly rotating star lacking significant magnetic field, the non-radial multiplets are nearly equally spaced in frequency space However, at moderate-to-fast rotations, stars deform more significantly into ellipsoids, causing the frequency spacing between adjacent azimuthal components to no longer remain constant. For the same reason, the $m = 0$ mode in some stars does not appear exactly mid-way between the $m = \pm 1$ components. The position of the $m = 0$ mode relative to the $m = \pm 1$ doublets is sensitive to stellar distortion. Even slight distortions in distant stars contain seismic imprints, allowing us to draw inferences (Gizon et al. 2016).

As in equation 2, rotation and magnetism shift the $m = 0$ mode by the amount $-2a_2$ relative to the cen-

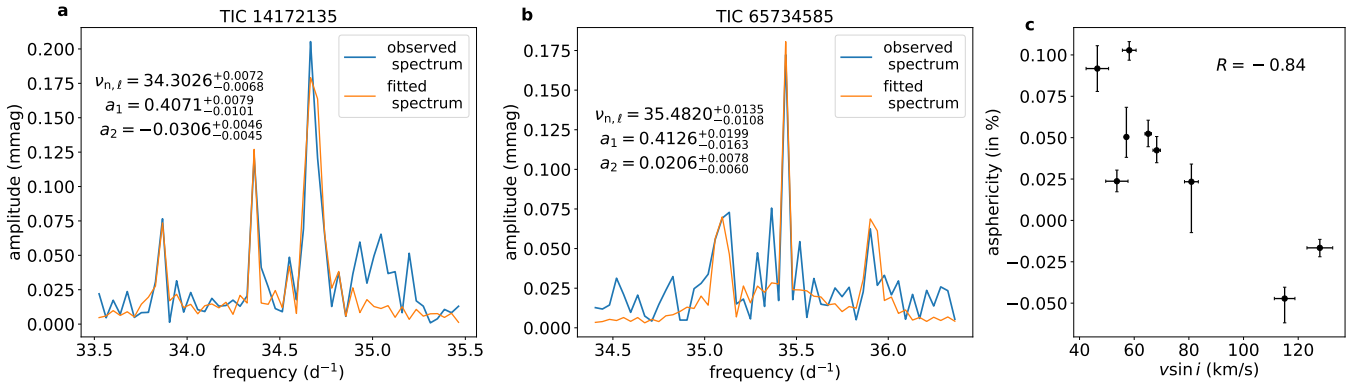

Figure 2. Ellipsoidal deformation measured in a δ Scuti star. a. Dipole-mode ($\ell = 1$) triplet in the frequency spectrum of TIC 14172135. Fitting the power spectrum with an appropriate formula, the central frequency ($\nu_{n,\ell}$) and coefficients a_1 and a_2 were obtained, as shown in the inset. All quantities are in d^{-1} units. Because $a_2 < 0$ for this star, the $m = 0$ component appears closer to the $m = +1$ component. **b.** Similar dipole-mode splitting observed in TIC 65734585, but the $m = 0$ mode is positioned closer to the $m = -1$ component, as a consequence of $a_2 > 0$. **c.** Asphericity - the relative difference between equatorial and polar radii - plotted against the line-of-sight projected rotational velocity ($v \sin i$).

(**Figure set-2 available with the MCMC convergence plots obtained from fitting the rotational splittings in 15 stars.**)

tral frequency $\nu_{n,\ell}$, while the $m = \pm 1$ components are displaced by $a_2 \pm a_1$ ($\approx \pm a_1$, since $|a_2| \ll a_1$). The coefficient a_2 captures the asymmetry in the position of the $m = 0$ component relative to the mean of the $m = \pm 1$ doublets (equation A11). Hence, $a_2 < 0$ (oblate) for stars with the $m = 0$ component closer to the $m = +1$ mode and $a_2 > 0$ (prolate) for stars where the $m = 0$ peak is proximal to the $m = -1$ mode. Therefore, the position of the $m = 0$ mode serves as a gauge with which to infer distortions in stellar structure,

$$\frac{R_{\rm eq} - R_{\rm pole}}{R_{\rm eq}} = -\frac{3}{8\pi}\frac{(2\ell+3)a_2}{\nu_{n,\ell}}. \quad (3)$$

The observationally measured a_2 coefficient contains additive contributions from centrifugal distortion and equatorial magnetic fields. The centrifugal component of a_2 is always a negative quantity (equation A9), whereas the contribution from magnetic activity can assume positive values (Benomar et al. 2023, equation 14). Thus positive a_2 values are suggestive of magnetic activity in the star, substantial enough to dominate the centrifugal effect. Cool stars, characterized by thick convective envelopes, generate dynamo magnetic fields and frequently exhibit such activity.

While centrifugal force and tidal interactions cause equatorial-bulging in stars, making them oblate, toroidal magnetic field can counteract this effect turning them prolate (Wentzel 1961). Precise frequency analysis suggests a prolate shape for 16 Cyg A (Bazot, M. et al. 2019). KIC 11145123, a γ Dor-δ Scuti hybrid, has been observed to be less oblate than expected from its centrifugal deformation alone, thereby indicating the presence of a near-equatorial magnetic field (Gizon et al. 2016).

Among the sample of 39 stars, 15 had visible $m = 0$ modes positioned between the $m = \pm 1$ multiplets. Fitting these triplets with equation 2, we obtained the a_1 and a_2 coefficients for those spectra. Our sample includes 9 stars with $a_2 < 0$ (oblate) and 6 stars with $a_2 > 0$ (prolate). We show one example of each type of distortion in Fig. 2 (a,b). The a_1 and a_2 coefficients calculated for these 15 stars are given in Table 1.

The deviation from sphericity for these stars, defined as $1 - R_{\rm pole}/R_{\rm eq}$ and calculated using equation 3, range from -0.05% (prolate) to +0.10% (oblate). These distortions are approximately ~ 100 times larger than that of KIC 11145123, a slowly rotating A type star, whose asphericity was measured to be $(1.8 \pm 0.6) \times 10^{-4}$% (Gizon et al. 2016). Deformations measured for the stars in our sample exceed ~ 100 times the Solar oblateness $(8.19 \pm 0.33) \times 10^{-4}$% (Meftah et al. 2015). While neither a_2 nor the asphericity showed any strong dependence on other observables, they exhibited a faint correlation with the spectroscopically measured $v \sin i$ (Fig. 2 c) – the latter being available for only 9 of the 15 stars (Sartoretti, P. et al. 2023). Pearson correlation coefficient R, which measures the linear correlation between these two quantities, is found to be -0.84 in this case. Asphericity takes positive values for oblate stars (equation 3), whereas for prolate objects it turns out negative. With the limited data presented here, stars appear to become prolate at larger rotation rates – which may be linked

to the generation of strong equatorial magnetic fields, capable of counteracting centrifugal deformation.

2.3. *Latitudinal Differential Rotation*

Échelle diagrams of δ Scuti stars often include ridges with modes that are not identified with degrees $\ell = 0$ or 1. These ridges are speculated to represent higher-degree ($\ell = 2$) harmonics (Bedding et al. 2020) of stellar oscillations. Quadrupolar modes form an additional ridge in the Échelle diagrams of δ Scuti stars immediately to the left of the ridge formed by the radial modes (Steindl, T. et al. 2022, Fig.2). Frequencies of quadrupolar ($\ell = 2$) multiplets are typically expressed in terms of the first four a-coefficients, as given in equation A13.

We visualized the Échelle diagrams of the 38 stars in our sample and found in one star (TIC 408165734) the potential presence of $\ell = 2$ multiplets, forming a cluster between the radial and dipole ridges (Fig. 3 a). One of the multiplets comprised four closely spaced modes which we interpreted to be $m = \{\pm1, \pm2\}$ modes (Fig. 3 c). The $m = 0$ mode is absent in this multiplet, which may be attributed either to a higher inclination angle or a (unknown) mode-suppressing mechanism.

Quadrupolar modes are the lowest angular-degree vibrations that may be used to infer the a_3 coefficient, a quantity that captures latitudinal rotational shear. This coefficient indicates the relative displacement between the centroids of $m = \pm1$ and $m = \pm2$ components (equation A12), and may be calculated from the frequencies of $m = \{\pm1, \pm2\}$ multiplets without requiring the $m = 0$ component.

In addition to the presence of quadrupole modes, this star exhibits a dipole doublet (Fig. 3c) – which also lacks the $m = 0$ mode, similar to the quadrupolar multiplets (Fig. 3d). The presence of the dipole mode in this star is very useful in cross-validating parameters obtained from these two independent groups of modes. Fitting the dipole modes with equation 2, we obtained $a_1 \approx 0.3307$ d^{-1}. Similarly, when fitted with equation A13, the quadrupolar modes yield the values $a_1 \approx 0.3196$ d^{-1} and $a_3 \approx 0.0367$ d^{-1}. The consistency between the values of the a_1 coefficients obtained from both the $\ell = 1$ and 2 multiplets suggests that our mode identifications of the quadruplets may be correct.

The positive sign of a_3 indicates that latitudinal shear in this star is solar-like, wherein the equator rotates faster than the pole. The ratio a_3/a_1 $\sim$10% in this star, suggesting that rotation in the envelopes of hot stars such as δ Scutis departs from constancy across their meridional cross-sections. In comparison, a_3 for the Sun is also approximately 10% of its mean rotation a_1. Self-consistent simulations (Espinosa Lara, F. & Rieutord, M. 2011) of rotation and meridional circulation in α Leo, a fast-rotating young star, indicate that it ought to show solar-like latitudinal shear and a companion meridional circulation of much smaller magnitude. Meridional flows play a crucial role in maintaining angular momentum balance and a latitudinal differential rotation profile cannot be maintained without this circulation (Hanasoge 2022).

3. DISCUSSION

Six δ Scuti stars that we examined exhibit asymmetry $a_2 > 0$, associated with prolate deformation (although at the level of 1-σ confidence). To estimate the magnetic field necessary to produce such frequency asymmetry, we assume rigid rotation and uniform magnetic field B. Using the formulation provided in equation B15, we obtained $B \sim 10^7$ Gauss for all the prolate stars, too large for a surface-localized field (Lampens, P. et al. 2013; Thomson-Paressant et al. 2023). Guo et al. (2024) also found that frequency shift in δ Scuti star due to magnetic fields as large as 10^5 Gauss (typically found in Red Giant cores) is smaller than the second order effect of rotational perturbation. Our assumption of a uniform magnetic field throughout the star is unrealistic, as its amplitude must decrease radially outwards. It is plausible that these stars harbor large magnetic fields in their convective cores, which may induce the prolate-like splittings in the modes.

APPENDIX

A. THEORY OF NON-RADIAL MODE SPLITTING

Rotation, centrifugal deformation, and magnetic activity – collectively break the frequency degeneracy between the multiplets of non-radial stellar oscillation modes. The impact of magnetic activity (Gizon 2002) on oscillation frequency depends on the field geometry, and its analysis remains beyond the scope of the current study. Nevertheless, rotation (Hansen et al. 1977) and centrifugal deformation (Gough & Thompson 1990) perturb the degenerate mode frequency in a simpler manner – as given in equations A1 and A2,

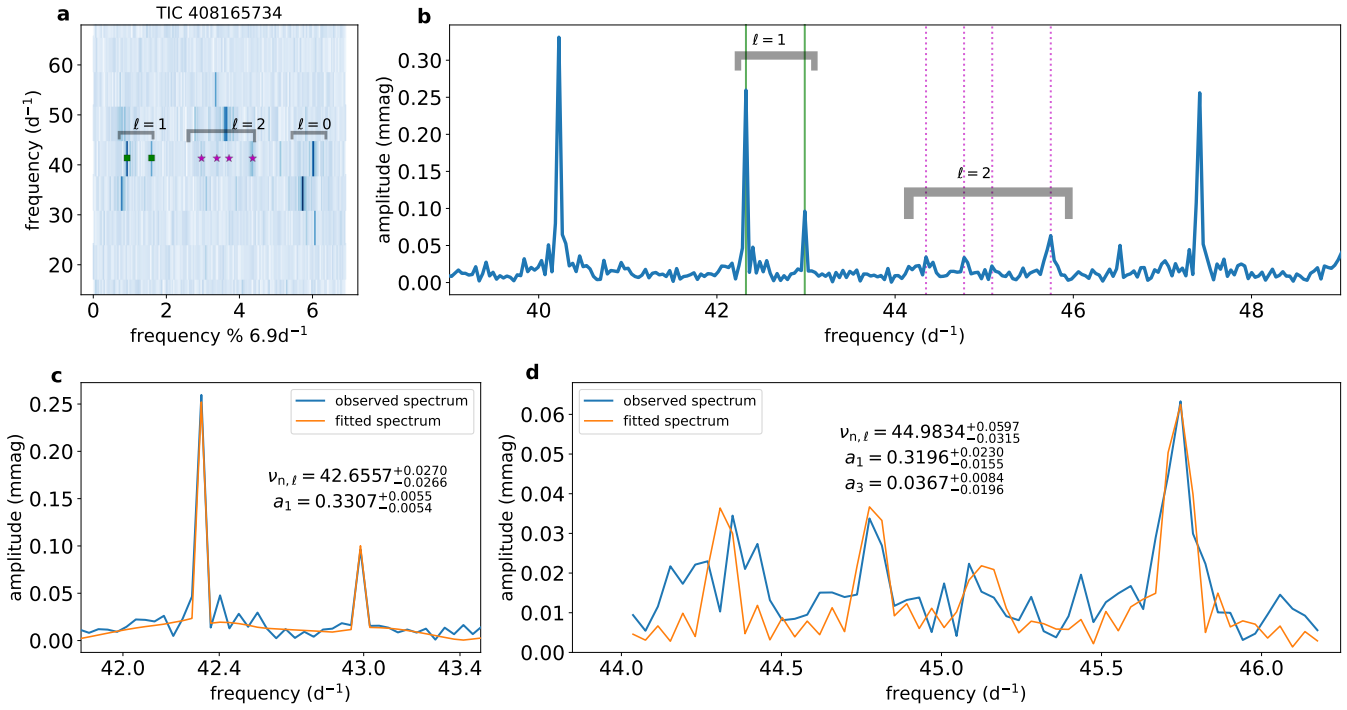

Figure 3. Inferring latitudinal differential rotation in a δ Scuti star. a. Échelle diagram of TIC 408165734, a star potentially harboring quadrupolar ($\ell = 2$) modes. The ridge on the right comprises radial ($\ell = 0$) modes, and the one on the left appears to be formed by dipole ($\ell = 1$) modes. We attribute the multiplet-like structure, midway between these two ridges, to quadrupolar modes. **b.** Oscillation spectrum of the star, with dipole and quadrupole modes marked using solid and dotted lines. **c.** Frequency spectrum of the same star in the $42.0 - 43.0\mathrm{d}^{-1}$ range showing a dipole doublet. We fitted this segment of the spectrum to obtain the relevant coefficients, as depicted in the plot in d^{-1} units. **d.** The spectrum within $44.0 - 46.0\mathrm{d}^{-1}$ shows a quadrupolar ($\ell = 2$) multiplet with four visible components. The fitted coefficients are given along with the plot. The a_1 coefficient, indicative of mean stellar rotation, is consistent with that derived from the dipole mode.

(**Figure set-3 available with the MCMC convergence plots obtained from fitting the dipole and quadrupole mode splitting in this star.**)

$$\nu_{\mathrm{n},\ell,\mathrm{m}} = \nu_{\mathrm{n},\ell} + \delta\nu^{\mathrm{rot}} + \delta\nu^{\mathrm{cf}} + \delta\nu^{\mathrm{act}},$$

$$\begin{aligned}\delta\nu^{\mathrm{rot}} &= (1 - C_L)\langle f_{\mathrm{rot}}\rangle \\ &= (1 - C_L) \oint K_{n,\ell}(\vec{r}) f_{\mathrm{rot}}(\vec{r}) d^3\vec{r}, \end{aligned} \tag{A1}$$

$$\delta\nu^{\mathrm{cf}} = \frac{2}{3}\frac{\ell(\ell+1) - 3m^2}{(2\ell-1)(2\ell+3)}\frac{\Omega^2 R^3}{GM}\nu_{\mathrm{n},\ell}, \tag{A2}$$

where (M, R, Ω) denote the stellar mass, radius, and mean rotation. The Ledoux constant C_L (Ledoux 1951) and the rotation-sensitivity kernel ($K_{\mathrm{n},\ell}$) of the oscillation modes are given below in terms of the horizontal and vertical displacements ($\xi_h(\vec{r}), \xi_r(\vec{r})$) and the density profile, $\rho(\vec{r})$.

$$C_L = \frac{\oint \rho\, \xi_h(2\xi_r + \xi_h) d\vec{r}}{\oint \rho\, [\xi_r^2 + \ell(\ell+1)\xi_h^2] d\vec{r}}, \tag{A3}$$

$$K_{n,\ell} = \frac{\rho\, [\xi_r^2 + \ell(\ell+1)\xi_h^2 - 2\xi_r\xi_h - \xi_h^2]}{\oint \rho\, [\xi_r^2 + \ell(\ell+1)\xi_h^2 - 2\xi_r\xi_h - \xi_h^2] d\vec{r}}. \tag{A4}$$

Given the average rotation $\langle f_{\mathrm{rot}}\rangle$ measured from the frequency splittings at multiple radial orders (n), the spatially resolved radial rotation profile may be inferred by inverting the kernel-weighted rotational splitting (equation A5) discretized over a grid of points (r^i) radially spanning from the centre to the stellar surface with spacing Δr.

$$\langle f_{\rm rot}\rangle_{n,\ell} = \sum_{i=1}^{N_{\rm grid}} K_{{\rm n},\ell}(r^i) f_{\rm rot}(r^i)\Delta r. \tag{A5}$$

The Coriolis effect alone does not affect the frequency of the $m = 0$ mode - it shifts the $\pm|m|$ modes symmetrically in opposite directions relative to the $m = 0$ mode. However, centrifugal distortion and magnetic activity perturb the $m = 0$ frequency as well and shift the $\pm|m|$ modes in the same direction (hence asymmetrically with respect to the $m = 0$ component). Therefore, the mathematical form of rotational frequency perturbations involve odd-only powers of m, while centrifugal deformation and magnetic activity involve even powers of m. Hence, the combined frequency perturbations are expressed as a common polynomial expansion (equation 1) in the basis of ζ functions multiplied by certain stellar-structure-dependent quantities known as a-coefficients.

Rotation-induced perturbations (symmetric in m, Ritzwoller & Lavely 1991) are written in terms of the odd a-coefficients (equation A6),

$$\delta\nu^{\rm rot} = \sum_{k=1}^{\ell} a_{2k-1}\ \zeta^{(\ell)}_{2k-1}(m). \tag{A6}$$

The first element of this series, the a_1 coefficient, is a measure of mean stellar rotation (Appourchaux, T. et al. 2014), and it may be estimated through the help of $\ell = 1$ modes alone. Similarly, the a_3 coefficient probes the extent of latitudinal differential rotation, where spin rates vary across layers from equator to pole, and it is only determined with modes of degrees $\ell \geq 2$.

Frequency splittings involving centrifugal deformation, low-latitude magnetic activity, tidal deformation, stratification and temperature perturbations (Benomar et al. 2023) are written in terms of even a-coefficients (equation A7),

$$\delta\nu^{\rm cf,act} = \sum_{s=1}^{\ell} a_{2s}\ \zeta^{(\ell)}_{2s}(m) \tag{A7}$$

$$a_{2s} = a^{\rm cf}_{2s} + a^{\rm act}_{2s} + a^{\rm tid}_{2s} + \cdots .$$

The first coefficient of this series, a_2, generally measures the deformation or asphericity (Gizon et al. 2016; Bazot, M. et al. 2019) of the stars, since the latter may be expressed through stellar structure and mode geometry (Gough & Thompson 1990) in accordance to

$$\frac{R_{\rm eq} - R_{\rm pole}}{R_{\rm eq}} = \frac{3}{8\pi}\beta_0 = \frac{3}{8\pi}\frac{\beta_{n,\ell,m}}{Q_{\ell,m}\ \nu_{{\rm n},\ell}}, \tag{A8}$$

which may be reduced to a function involving the a_2-coefficient alone (equation 3) by substituting

$$\beta_{n,\ell,m} = a_2^{n,\ell}\zeta_2^{(\ell)} = \frac{3m^2 - \ell(\ell+1)}{(2\ell-1)}a_2^{n,\ell},$$

and

$$Q_{\ell,m} = \frac{\ell(\ell+1) - 3m^2}{(2\ell-1)(2\ell+3)}.$$

The coefficient a_2 may be inferred only if the $m = 0$ component of any non-radial mode is visible in the spectrum of the star. The centrifugal component of a_2 (Benomar et al. 2023, equation 12) may be expressed in terms of mass, radius, stellar rotation and frequency of the unperturbed central mode (equation A9),

$$a_2^{\rm cf} = -\frac{1}{2\ell+3}\frac{\Omega^2 R_\star^3}{GM_\star}\nu_{{\rm n},\ell}. \tag{A9}$$

However, the a_2 contribution from magnetic activity is not easily written in a simple analytical form (Benomar et al. 2023, equation 14), since it depends on the specific magnetic-field geometry.

It is straightforward to extract the three leading a-coefficients, provided the frequencies of non-radial multiplets are precisely determined (Benomar et al. 2023, eq. A.8, A.9, A.12),

$$a_1 = \frac{\nu_{\mathrm{n},1,+1} - \nu_{\mathrm{n},1,-1}}{2}, \tag{A10}$$

$$a_2 = \frac{\frac{\nu_{\mathrm{n},1,+1} + \nu_{\mathrm{n},1,-1}}{2} - \nu_{\mathrm{n},1,0}}{3}, \tag{A11}$$

$$a_3 = \frac{\frac{\nu_{\mathrm{n},2,+2} - \nu_{\mathrm{n},2,-2}}{4} - \frac{\nu_{\mathrm{n},2,+1} - \nu_{\mathrm{n},2,-1}}{2}}{5}. \tag{A12}$$

A non-radial mode of degree ℓ may be used to determine a-coefficients up to $a_{2\ell}$. Since a majority of the δ Scuti stars predominantly pulsate in $\ell = 0$ and 1 modes, it is possible to obtain a_1 and a_2 for most of them, the latter being measurable only when $m = 0$ modes are observable. Occasionally, these stars also exhibit quadrupolar ($\ell = 2$) oscillations, in which case, it may be possible to retrieve their a_3 coefficients. In this case, frequencies of the quadrupolar multiplets may be expressed as follows.

$$\nu_{n,2,m} = \nu_{n,2} + a_1 m + a_2(m^2 - 2) + a_3\left(\frac{5m^3 - 17m}{3}\right) + a_4\left(\frac{35m^4 - 155m^2 + 72}{6}\right) \tag{A13}$$

B. INFERENCE OF MAGNETIC FIELD

Incorporating both the first- and second-order rotational splittings (Suárez et al. 2006) alongside the perturbation induced by the magnetic field (Mathis et al. 2021; Guo et al. 2024), the complete expression for the frequency of the p-mode oscillation may be formulated as shown in equation B14,

$$\omega_{n,\ell,m} = \omega_c + m(1 - C_L)\Omega + \frac{\ell(\ell+1) - 3m^2}{4\ell(\ell+1) - 3}\mathcal{J}_c\frac{\Omega^2}{\omega_c} + D_{\ell,m}\frac{\int_0^R \frac{B^2}{4\pi\rho c^2}\frac{dr}{c}}{\int_0^R \frac{dr}{c}}\omega_c, \tag{B14}$$

where C_L is the Ledoux constant defined in equation A3, ω_c the unperturbed mode frequency, ρ the interior density profile, and c the sound speed. $D_{\ell,m}$ is an integral involving spherical harmonics (Mathis et al. 2021), with values $\frac{4}{5}$ for $m = \pm 1$ and $\frac{2}{5}$ for the $m = 0$ component of the dipole ($\ell = 1$) modes. $\mathcal{J}_c$ is an integral encompassing several quantities associated with stellar structure (Suárez et al. 2006).

Using equation A11, the dipole mode asymmetry a_2 may be written as

$$2\pi a_2 = \frac{0.5(\omega_{n,1,+1} + \omega_{n,1,-1}) - \omega_{n,1,0}}{3} = -\frac{1}{5}\mathcal{J}_c\frac{\Omega^2}{\omega_c} + \frac{2}{15}\frac{\int_0^R \frac{B^2}{4\pi\rho c^2}\frac{dr}{c}}{\int_0^R \frac{dr}{c}}\omega_c,$$

which may be solved for uniform toroidal magnetic field

$$B^2 = 12\pi^2\frac{\int_0^R \frac{dr}{c}}{\int_0^R \frac{dr}{\rho c^3}}\left(5\frac{a_2}{\omega_c} + 2\mathcal{J}_c\frac{a_1^2}{\omega_c^2}\right)m, \tag{B15}$$

with the substitution $\Omega = 2\pi a_1$.

C. FITTING THE OSCILLATION SPECTRA

The oscillation spectrum of a non-radial mode of degree ℓ may be modeled through a set of parameters θ – the central frequency $\nu_{\mathrm{n},\ell}$, a-coefficients $\{a_i | 1 \leq i \leq 2\ell\}$, mode amplitudes h_m, and mode widths w_m. These parameters may be used to build the spectrum by constructing sinc profiles (equation C16) around each multiplet frequency ($\nu_{\mathrm{n},\ell,\mathrm{m}}$) generated by the equation 2 and A13.

$$S_{\rm model}(\theta) = \sum_{m=-\ell}^{\ell} h_m \ {\rm sinc}\left(\frac{\nu - \nu_{{\rm n},\ell,{\rm m}}}{w_m/2}\right) \tag{C16}$$

We used the Python package `Dynesty` (Speagle 2020; Koposov et al. 2024) to fit the multiplet frequencies and obtain the posterior distributions of the relevant parameters. For all parameters θ, we chose a uniform prior (equation C17) by dynamically deciding their appropriate bounds. A Gaussian likelihood function (equation C18) was used to determine how well the spectrum generated by a set of parameters θ fits the observed spectrum $S_{\rm obs}$, given the noise level σ determined by its median. The posterior distribution of the fitted parameters can be obtained by multiplying the likelihood with the prior (equation C19). The algorithm samples the parameter space of interest according to the posterior probability, and the resulting parameter distribution provides the best-fit solutions along with the uncertainties.

$$P(\theta) = U(\theta; a, b) \tag{C17}$$

$$\mathcal{L}(S_{\rm obs}|\theta) = e^{-\frac{1}{2}\left(\frac{S_{\rm obs} - S_{\rm model}(\theta)}{\sigma}\right)^2} \tag{C18}$$

$$P(\theta|S_{\rm obs}) = \mathcal{L}(S_{\rm obs}|\theta)\ P(\theta) \tag{C19}$$

D. FORWARD MODELING OF ROTATIONAL SPLITTING

We attempted to fit an empirical three-parameter rotation model to explain the four rotational splittings observed in the oscillation spectrum of TIC 307930890. We applied the MCMC sampler `Dynesty` (Speagle 2020) to optimize the spin parameters $\{\Omega\}$ representing an array of rotation rates at positions $r = 0.91, 0.95, 0.99 R_\star$. Solving four linear equations comprising three independent degrees of freedom ensures the uniqueness of the obtained solution.

We chose a uniform prior between appropriate ranges for each of the three rotation parameters (equation D20). Given the set of parameters $\{\Omega\}$, rotational splitting ($\delta\nu_j^{\rm model}$) at different radial orders j were obtained using equation A1. The probabilities of these parameters regenerating the observed mode-splittings were calculated using a Gaussian likelihood function of the differences between the observed and modelled splittings scaled by the uncertainties $\sigma_j^{\rm obs}$ (equation D21). `Dynesty` samples the three-dimensional $\{\Omega\}$ space following the posterior probability obtained by the product of the likelihood and the prior functions (equation D22). The statistics of the parameters traced by the MCMC sampler indicate how likely they fit the observed rotational splittings,

$$P(\Omega) = U(\Omega; 0.1 - 0.9{\rm d}^{-1}) \tag{D20}$$

$$\mathcal{L}(\delta\nu^{\rm obs}|\Omega) = e^{-\frac{1}{2}\sum_{j=3}^{6}\left(\frac{\delta\nu_j^{\rm obs} - \delta\nu_j^{\rm model}(\Omega)}{\sigma_j^{\rm obs}}\right)^2} \tag{D21}$$

$$P(\Omega|\delta\nu^{\rm obs}) = \mathcal{L}(\delta\nu^{\rm obs}|\Omega)\ P(\Omega). \tag{D22}$$

Acknowledgments: This work has made use of the SIMBAD and VizieR databases. We are thankful for the valuable data released by the NASA's TESS mission and the European Space Agency (ESA) space mission Gaia. We applied `Lightkurve` (Lightkurve Collaboration 2018), a Python package for analyzing the Kepler and TESS data. We acknowledge support from the DAE, Government of India (grant no. RTI 4002). All computations were performed in the Intel Lab Academic Compute Environment. We used the `MESA` and `GYRE` codes available at Zenodo: doi:10.5281/zenodo.13879880. This research was supported in part by a generous donation (from the Murty Trust) aimed at enabling advances in astrophysics through the use of machine learning. Murty Trust, an initiative of the Murty Foundation, is a not-for-profit organisation dedicated to the preservation and celebration of culture, science, and knowledge systems born out of India. The Murty Trust is headed by Mrs. Sudha Murty and Mr. Rohan Murty.

REFERENCES

Aerts, C., Christensen-Dalsgaard, J., & Kurtz, D. 2010, Asteroseismology, Astronomy and Astrophysics Library (Springer Netherlands). https://ui.adsabs.harvard.edu/abs/2010aste.book.....A

Appourchaux, T., Antia, H. M., Benomar, O., et al. 2014, A&A, 566, A20, doi: 10.1051/0004-6361/201323317

Star	$\Delta\nu$ (d^{-1})	a_1 (d^{-1})	a_2 (d^{-1})	$\frac{R_{eq}-R_{pol}}{R_{eq}}$ (%)	v sin i (km s^{-1})
TIC 14172135	6.426 ± 0.328	$0.4071^{+0.0079}_{-0.0101}$	$-0.0306^{+0.0046}_{-0.0045}$	$+0.0532^{+0.0080}_{-0.0078}$	65.116 ± 1.191
TIC 30624832	6.659 ± 0.221	$0.4149^{+0.1074}_{-0.0262}$	$+0.0174^{+0.0112}_{-0.0321}$	$-0.0485^{+0.0312}_{-0.0896}$	
TIC 42827654	7.061 ± 0.540	$0.3086^{+0.0046}_{-0.0037}$	$-0.0260^{+0.0051}_{-0.0046}$	$+0.0423^{+0.0083}_{-0.0075}$	68.227 ± 1.364
TIC 59365685	6.731 ± 0.252	$0.3309^{+0.0094}_{-0.0094}$	$-0.0141^{+0.0040}_{-0.0038}$	$+0.0236^{+0.0067}_{-0.0063}$	53.657 ± 4.080
TIC 65734585	6.889 ± 0.298	$0.4126^{+0.0199}_{-0.0163}$	$+0.0206^{+0.0078}_{-0.0060}$	$-0.0346^{+0.0131}_{-0.0101}$	
TIC 111840813	6.583 ± 0.325	$0.3387^{+0.0055}_{-0.0084}$	$-0.0287^{+0.0102}_{-0.0070}$	$+0.0504^{+0.0179}_{-0.0123}$	57.139 ± 0.670
TIC 165674519	6.629 ± 0.334	$0.3549^{+0.0200}_{-0.0660}$	$-0.0162^{+0.0074}_{-0.0213}$	$+0.0233^{+0.0106}_{-0.0307}$	80.922 ± 2.532
TIC 177715827	7.500 ± 0.226	$0.4364^{+0.0165}_{-0.0189}$	$+0.0153^{+0.0068}_{-0.0064}$	$-0.0170^{+0.0075}_{-0.0071}$	
TIC 238641255	7.174 ± 0.293	$0.5505^{+0.0100}_{-0.0109}$	$+0.0142^{+0.0044}_{-0.0046}$	$-0.0165^{+0.0051}_{-0.0053}$	127.918 ± 4.714
TIC 307930890	7.212 ± 0.268	$0.4207^{+0.0034}_{-0.0039}$	$-0.0335^{+0.0371}_{-0.0288}$	$+0.0389^{+0.0431}_{-0.0334}$	
TIC 365852391	6.867 ± 0.206	$0.4554^{+0.0132}_{-0.0374}$	$+0.0393^{+0.0057}_{-0.0122}$	$-0.0472^{+0.0068}_{-0.0146}$	115.039 ± 3.771
TIC 377257563	5.906 ± 0.367	$0.4470^{+0.0082}_{-0.0096}$	$-0.0386^{+0.0058}_{-0.0058}$	$+0.0917^{+0.0138}_{-0.0138}$	46.508 ± 4.124
TIC 405483817	6.980 ± 0.228	$0.2964^{+0.0130}_{-0.0858}$	$-0.0323^{+0.0083}_{-0.0110}$	$+0.0540^{+0.0139}_{-0.0185}$	
TIC 423159418	6.837 ± 0.270	$0.4470^{+0.0172}_{-0.0530}$	$+0.0086^{+0.0074}_{-0.0173}$	$-0.0119^{+0.0102}_{-0.0240}$	
TIC 47639058	4.880 ± 0.200	$0.4417^{+0.0097}_{-0.0067}$	$-0.0689^{+0.0035}_{-0.0040}$	$+0.1028^{+0.0052}_{-0.0059}$	58.183 ± 2.509
Sun	11.681 ± 0.021	0.0363 ± 0.0008		$+0.0008 \pm 0.00003$	1.971 ± 0.003

Table 1. Large frequency separation ($\Delta\nu$), the first two a-coefficients, structural deformations, and $v \sin i$ (Sartoretti, P. et al. 2023) for the 15 stars we studied in section 2.2. We also provide the corresponding solar values (Balthasar 1984; Benomar et al. 2023) for the sake of comparison. While $\Delta\nu$ acts as a proxy for mean stellar density (Suárez, J. C. et al. 2014), the a_1 and a_2 coefficients measure mean rotation and structure deformation, respectively.

Balona, L. A. 2019, Monthly Notices of the Royal Astronomical Society, 490, 2112, doi: 10.1093/mnras/stz2808

Balthasar, H. 1984, SoPh, 93, 219, doi: 10.1007/BF02270836

Bazot, M., Benomar, O., Christensen-Dalsgaard, J., et al. 2019, A&A, 623, A125, doi: 10.1051/0004-6361/201834594

Bedding, T. R., Murphy, S. J., Hey, D. R., et al. 2020, Nature, 581, 147, doi: 10.1038/s41586-020-2226-8

Belkacem, K., Marques, J. P., Goupil, M. J., et al. 2015, A&A, 579, A30, doi: 10.1051/0004-6361/201526042

Benomar, O., Takata, M., Bazot, M., et al. 2023, Astronomy & Astrophysics, 680, A27, doi: 10.1051/0004-6361/202347095

Benomar, O., Takata, M., Shibahashi, H., Ceillier, T., & García, R. A. 2015, Monthly Notices of the Royal Astronomical Society, 452, 2654, doi: 10.1093/mnras/stv1493

Benomar, O., Bazot, M., Nielsen, M. B., et al. 2018, Science, 361, 1231–1234, doi: 10.1126/science.aao6571

Bowman, D. M. 2020, Frontiers in Astronomy and Space Sciences, 7, doi: 10.3389/fspas.2020.578584

Cantiello, M., Mankovich, C., Bildsten, L., Christensen-Dalsgaard, J., & Paxton, B. 2014, The Astrophysical Journal, 788, 93, doi: 10.1088/0004-637X/788/1/93

Damiani, C., & Mathis, S. 2018, A&A, 618, A90, doi: 10.1051/0004-6361/201732538

Espinosa Lara, F., & Rieutord, M. 2011, A&A, 533, A43, doi: 10.1051/0004-6361/201117252

Fuller, J., Lecoanet, D., Cantiello, M., & Brown, B. 2014, The Astrophysical Journal, 796, 17, doi: 10.1088/0004-637X/796/1/17

Fuller, J., Piro, A. L., & Jermyn, A. S. 2019, Monthly Notices of the Royal Astronomical Society, 485, 3661, doi: 10.1093/mnras/stz514

Gagnier, D., Rieutord, M., Charbonnel, C., Putigny, B., & Espinosa Lara, F. 2019, A&A, 625, A88, doi: 10.1051/0004-6361/201834599

Gizon, L. 2002, Astronomische Nachrichten, 323, 251. https://ui.adsabs.harvard.edu/abs/2002AN....323..251G

Gizon, L., Sekii, T., Takata, M., et al. 2016, Science Advances, 2, doi: 10.1126/sciadv.1601777

Goldstein, J., & Townsend, R. H. D. 2020, The Astrophysical Journal, 899, 116, doi: 10.3847/1538-4357/aba748

Gough, D. O., & Thompson, M. J. 1990, Monthly Notices of the Royal Astronomical Society, 242, 25, doi: 10.1093/mnras/242.1.25

Guo, Z., Bedding, T. R., Pamyatnykh, A. A., et al. 2024, Monthly Notices of the Royal Astronomical Society, 535, 2927, doi: 10.1093/mnras/stae2423

Guzik, J. A. 2021, Frontiers in Astronomy and Space Sciences, 8, doi: 10.3389/fspas.2021.653558

Hanasoge, S. M. 2022, Living Reviews in Solar Physics, 19, doi: 10.1007/s41116-022-00034-7

Hansen, C. J., Cox, J. P., & van Horn, H. M. 1977, ApJ, 217, 151, doi: 10.1086/155564

Hastings, B., Langer, N., & Puls, J. 2023, A&A, 672, A60, doi: 10.1051/0004-6361/202245281

Hastings, B., Langer, N., Wang, C., Schootemeijer, A., & Milone, A. P. 2021, A&A, 653, A144, doi: 10.1051/0004-6361/202141269

Koenigsberger, G., Moreno, E., & Langer, N. 2021, A&A, 653, A127, doi: 10.1051/0004-6361/202039369

Koposov, S., Speagle, J., Barbary, K., et al. 2024, joshspeagle/dynesty: v2.1.4, v2.1.4, Zenodo, doi: 10.5281/zenodo.12537467

Kurtz, D. W., Saio, H., Takata, M., et al. 2014, Monthly Notices of the Royal Astronomical Society, 444, 102, doi: 10.1093/mnras/stu1329

Lampens, P., Tkachenko, A., Lehmann, H., et al. 2013, A&A, 549, A104, doi: 10.1051/0004-6361/201219525

Ledoux, P. 1951, ApJ, 114, 373, doi: 10.1086/145477

Lightkurve Collaboration. 2018, Lightkurve: Kepler and TESS time series analysis in Python, Astrophysics Source Code Library. http://ascl.net/1812.013

Machida, M. N., ichiro Inutsuka, S., & Matsumoto, T. 2007, The Astrophysical Journal, 670, 1198, doi: 10.1086/521779

Mathis, S., Bugnet, L., Prat, V., et al. 2021, Astronomy & Astrophysics, 647, A122, doi: 10.1051/0004-6361/202039180

Meftah, M., Irbah, A., Hauchecorne, A., et al. 2015, Solar Physics, 290, 673–687, doi: 10.1007/s11207-015-0655-6

Mosser, B., Goupil, M. J., Belkacem, K., et al. 2012, A&A, 548, A10, doi: 10.1051/0004-6361/201220106

Paxton, B., Bildsten, L., Dotter, A., et al. 2010, The Astrophysical Journal Supplement Series, 192, 3, doi: 10.1088/0067-0049/192/1/3

Paxton, B., Cantiello, M., Arras, P., et al. 2013, The Astrophysical Journal Supplement Series, 208, 4, doi: 10.1088/0067-0049/208/1/4

Paxton, B., Marchant, P., Schwab, J., et al. 2015, The Astrophysical Journal Supplement Series, 220, 15, doi: 10.1088/0067-0049/220/1/15

Paxton, B., Schwab, J., Bauer, E. B., et al. 2018, The Astrophysical Journal Supplement Series, 234, 34, doi: 10.3847/1538-4365/aaa5a8

Paxton, B., Smolec, R., Schwab, J., et al. 2019, The Astrophysical Journal Supplement Series, 243, 10, doi: 10.3847/1538-4365/ab2241

Reeth, T. V., Tkachenko, A., Aerts, C., et al. 2015, The Astrophysical Journal Supplement Series, 218, 27, doi: 10.1088/0067-0049/218/2/27

Ritzwoller, M. H., & Lavely, E. M. 1991, ApJ, 369, 557, doi: 10.1086/169785

Sartoretti, P., Marchal, O., Babusiaux, C., et al. 2023, A&A, 674, A6, doi: 10.1051/0004-6361/202243615

Schou, J., Christensen-Dalsgaard, J., & Thompson, M. J. 1994, ApJ, 433, 389, doi: 10.1086/174653

Song, H. F., Wang, J. Z., Song, F., & Wang, J. T. 2017, A&A, 600, A42, doi: 10.1051/0004-6361/201629784

Speagle, J. S. 2020, Monthly Notices of the Royal Astronomical Society, 493, 3132–3158, doi: 10.1093/mnras/staa278

Steindl, T., Zwintz, K., & Müllner, M. 2022, A&A, 664, A32, doi: 10.1051/0004-6361/202243242

Suárez, J. C., Goupil, M. J., & Morel, P. 2006, Astronomy & Astrophysics, 449, 673–685, doi: 10.1051/0004-6361:20054181

Suárez, J. C., García Hernández, A., Moya, A., et al. 2014, A&A, 563, A7, doi: 10.1051/0004-6361/201322270

Thomson-Paressant, K., Neiner, C., Lampens, P., et al. 2023, Monthly Notices of the Royal Astronomical Society, 526, 1728, doi: 10.1093/mnras/stad2798

Townsend, R. H. D., Goldstein, J., & Zweibel, E. G. 2017, Monthly Notices of the Royal Astronomical Society, 475, 879, doi: 10.1093/mnras/stx3142

Townsend, R. H. D., & Teitler, S. A. 2013, Monthly Notices of the Royal Astronomical Society, 435, 3406, doi: 10.1093/mnras/stt1533

von Zeipel, H. 1924, mnras, 84, 665, doi: 10.1093/mnras/84.9.665

Wentzel, D. G. 1961, ApJ, 133, 170, doi: 10.1086/147014

Zahn, J.-P., Brun, A. S., & Mathis, S. 2007, A&A, 474, 145, doi: 10.1051/0004-6361:20077653

Zwintz, K., Neiner, C., Kochukhov, O., et al. 2020, A&A, 643, A110, doi: 10.1051/0004-6361/202038210